AirLLM: Diffusion Policy-based Adaptive LoRA for Remote Fine-Tuning of LLMs over the Air

Shiyi Yang, Xiaoxue Yu, Rongpeng Li, Jianhang Zhu, Zhifeng Zhao, Honggang Zhang

arXiv:2507.11515v2 [cs.LG] 27 Aug 2026

***Abstract*—Operating Large Language Models (LLMs) on edge devices is increasingly challenged by limited communication bandwidth and strained computational and memory costs. Thus, cloud-assisted remote fine-tuning becomes indispensable. Nevertheless, existing Low-Rank Adaptation (LoRA) approaches typically employ fixed or heuristic rank configurations, and the subsequent over-the-air transmission of all LoRA parameters could be rather inefficient. To address this limitation, we develop AirLLM, a hierarchical diffusion policy framework for communication-aware LoRA adaptation. Specifically, AirLLM models the rank configuration as a structured action vector that spans all LoRA-inserted projections. To solve the underlying high-dimensional sequential decision-making problem, a Proximal Policy Optimization (PPO) agent generates coarse-grained decisions by jointly observing wireless states and linguistic complexity, which are then refined via a Denoising Diffusion Implicit Model (DDIM) to produce high-resolution, task- and channel-adaptive rank vectors. The two modules are optimized alternatively, with the DDIM trained under the Classifier-Free Guidance (CFG) paradigm to maintain alignment with PPO rewards. Experiments under varying signal-to-noise ratios demonstrate that AirLLM consistently enhances fine-tuning performance while significantly reducing transmission costs, highlighting the effectiveness of reinforcement-driven, diffusion-refined rank adaptation for scalable and efficient remote fine-tuning over the air.**

***Index Terms*—Remote Fine-Tuning, Diffusion Policy, Reinforcement Learning, Adaptive Low-Rank Adaptation.**

I. Introduction

Large Language Models (LLMs) have demonstrated strong generalization across a wide range of natural language processing tasks [1], [2]. However, their substantial parameter and memory footprints create major challenges for efficient deployment [3], especially on edge devices with limited computational and storage resources. Full fine-tuning of such large models entails enormous computational and memory demands, making it infeasible for on-device learning. To reduce these costs, Parameter-Efficient Fine-Tuning (PEFT) [4] methods such as Low-Rank Adaptation (LoRA) [5] and its adaptive variant AdaLoRA [6] decompose updates into low-rank matrices or dynamically allocate rank budgets based on Singular Value Decomposition (SVD). While effective in reducing computational load, they primarily focus on the training process itself, often overlooking the deployment constraints of real-world systems.

S. Yang, X. Yu, R. Li, and J. Zhu are with the College of Information Science and Electronic Engineering, Zhejiang University, Hangzhou 310027, China (e-mail: {12531136; sdwhyxx; lirongpeng; zhujh20}@zju.edu.cn).

Z. Zhao is with Zhejiang Lab, Hangzhou 310012, China, and also with Zhejiang University, Hangzhou 310027, China (e-mail: zhaozf@zhejianglab.com).

H. Zhang (e-mail: honggang.zhang@ieee.org).

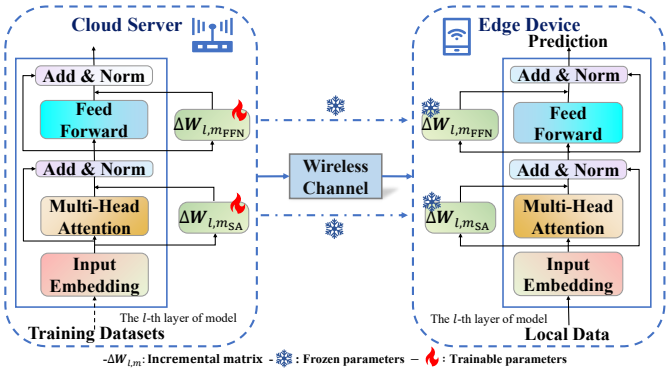

Fig. 1. An illustrative example of remote fine-tuning of an LLM over the air.

However, existing PEFT methods are poorly suited for remote fine-tuning under real-time wireless channel dynamics, since the reliance on static rank allocation and the ignorance of communication overhead leads to either redundant transmissions or insufficient performance. This limitation is further exacerbated in edge-cloud collaborative learning. Edge devices usually lack sufficient resources for local fine-tuning, and it is difficult to meet global end-to-end constraints such as the edge device latency limit. So model adaptation is mainly performed on cloud servers [7]. The updated parameters must be transmitted to the edge over wireless channels as illustrated in Fig. 1, which have limited bandwidth and fluctuating signal-to-noise ratio (SNR). Meanwhile, training data collected from different sources often exhibits diverse characteristics and complexities, such as high Out-Of-Vocabulary (OOV) rates or varying lexical entropy [8], indicating the vocabulary mismatch and linguistic variability. These factors directly affect the relative importance of different layers during adaptation. More critically, most existing transmission and compression techniques are designed independently from tuning strategies [9], leading to suboptimal trade-offs between communication cost and adaptation quality. Therefore, to overcome these limitations, efficient remote fine-tuning of LLMs [10] on the cloud and the transmission of partial, essential parameters to the edge emerge as a promising solution. Wireless channel configurations and propagation conditions, however, directly affect this transmission process [11]. In other words, only a subset of layers meaningfully contribute to downstream task performance, the allocated ranks are carefully calibrated for particular LLM projection, feed-forward network (FFN) [12], and output layers. Unfortunately, traditional heuristics such as greedy selection or fixed allocation [6] cannot directly account

for such dynamic, high-dimensional, and multi-objective requirements. This limitation becomes more pronounced when adaptation must track time-varying wireless channels [13].

To address these issues, we propose AirLLM, a communication-aware adaptive LoRA framework that dynamically adjusts layer-wise ranks based on real-time wireless channel conditions and fine-tuning dataset properties. By formulating high-dimensional rank allocation as a sequential decision-making problem under communication constraints, AirLLM leverages Reinforcement Learning (RL) [14] to learn adaptive rank allocation policies. The proposed RL agent observes both data and channel state information and dynamically adjusts rank budgets to balance model accuracy and transmission cost. In particular, SNR has been used as an adaptive input under dynamic channel conditions [15]. However, standard RL algorithms still struggle with the underlying high-dimensional action spaces. Therefore, due to high-dimensional modeling capability, we resort to the classifier-free denoising diffusion [16], [17]. Featuring the integration of semantic-channel aware state design, diffusion-based policy generation, and a multi-objective reward formulation, our proposed framework, **AirLLM**, resolves the mismatch between conventional PEFT methods and the practical requirements of wireless remote fine-tuning, obtaining balanced fine-tuning performance under bandwidth constraints.

Key contributions are as follows:

- **Formulating Remote Fine-Tuning as a Markov Decision Process Problem**: We propose a novel formulation of remote LLM fine-tuning as a Markov Decision Process (MDP), where each decision corresponds to a layer-wise low-rank configuration under resource constraints. To support effective policy learning, we design a comprehensive RL state space. It includes wireless channel statistics (e.g., SNR), data complexity metrics (e.g., lexical entropy, OOV rate) [8], and current rank assignments. Additionally, a multi-objective reward function is constructed to balance downstream task performance with communication efficiency, enabling the RL agent to adaptively optimize fine-tuning strategies in dynamic environments.
- **Hierarchical Diffusion Policy for Scalable Structured Action Generation**: To address the challenge of high-dimensional decision-making in layer-wise rank allocation, we propose a hierarchical policy framework that combines a lightweight Proximal Policy Optimization (PPO)-based coarse policy with a conditional Denoising Diffusion Implicit Model (DDIM) [18]-based refinement module. Instead of directly predicting discrete rank configurations, the PPO agent [19] outputs a continuous latent vector. This vector provides coarse layer-wise guidance for the DDIM sampler, which then refines the final structured rank vector across layers. Particularly, DDIM adopts the Classifier-Free Guidance (CFG) strategy to better align the denoising process with task rewards. Through training PPO and DDIM modules alternately, our approach significantly improves training stability and enables scalable action generation in large configuration spaces.
- **Extensive Experimental Validation and Efficiency Gains**: We conduct comprehensive experiments across multiple wireless communication scenarios and natural language understanding tasks to evaluate the effectiveness of our framework. Results demonstrate that compared to existing PEFT baselines [6], our method reduces parameter transmission costs by up to 12.5% while improving task accuracy by 0.69%. Moreover, the proposed Diffusion-RL hybrid framework achieves over 30% training efficiency gains compared to vanilla PPO [19], validating its practical applicability in real-world cloud-edge deployment settings.

This paper is organized as follows. Section II reviews related literature. Section III presents the system model and formulates the problem. Section IV details the proposed hierarchical model for fine-tuning. Section V evaluates performance via simulations. Finally, the main conclusion is drawn in Section VI.

II. Related Work

A. Parameter-Efficient Fine-Tuning for Large Language Models

The rapid advancement of LLMs has prompted an extensive investigation into PEFT methods, primarily motivated by the prohibitive cost of full-model updates in large-scale architectures. LoRA [5] pioneers this topic by replacing full fine-tuning with low-rank adaptation modules. Specifically, it approximates the update $\Delta\mathbf{W} \in \mathbb{R}^{m\times n}$ using two low-rank matrices $\mathbf{A} \in \mathbb{R}^{m\times r}$ and $\mathbf{B} \in \mathbb{R}^{r\times n}$, with $r \ll m, n$, significantly reducing trainable parameters while preserving downstream performance. However, LoRA and its early variants typically assign a uniform rank r across all layers and modules, neglecting the inherent heterogeneity in importance and complexity among different components [6], [20].

To address this limitation, AdaLoRA [6] dynamically adjusts rank allocation by estimating parameter importance during training. It employs heuristic criteria derived from the SVD of parameter matrices and gradient information to guide adaptive rank adjustment. Despite these improvements, its assumption of static data distributions and system environments implies a lack of explicit mechanisms to handle dynamic and noisy wireless channels that are typical in cloud-to-edge parameter transmission [21].

B. Adaptive Rank Allocation in Edge-Cloud Settings

Despite the progress in PEFT methods for high-performance environments, little attention has been paid to communication constraints when deploying fine-tuned parameters on resource-constrained edge devices. In edge-cloud collaborative learning, fine-tuning is commonly offloaded to cloud servers, necessitating the transmission of updated low-rank parameters over wireless channels with varying bandwidth and SNR [22], [23].

Recent systems such as dLoRA dynamically orchestrate requests and LoRA adapters to improve serving efficiency [24]. However, such serving-level optimization does not adapt fine-tuning ranks to wireless channel conditions or dataset

complexity. To address this gap, we formulate adaptive rank allocation as a sequential decision-making problem and leverage RL to jointly optimize rank assignments based on dataset characteristics (e.g., lexical entropy, OOV rates) and real-time channel states (e.g., SNR, bandwidth) [25].

C. Reinforcement Learning for Rank Adaptation

The integration of RL into PEFT for dynamic rank adaptation remains relatively under-explored. While conventional RL algorithms such as PPO [19] are theoretically applicable, they encounter practical challenges in large-scale Transformer-based LLMs. Specifically, assigning ranks across multiple Transformer blocks induces a high-dimensional action space, often resulting in inefficient learning and suboptimal policy performance [26], [27].

To mitigate this, latent-space policies and distributional RL have been studied for high-dimensional decision making [28], [29]. Diffusion policies further formulate policy generation as a denoising process for complex, structured action distributions [16], [30]. In our approach, we adopt the DDIM [18] for its accelerated inference compared to Denoising Diffusion Probabilistic Models (DDPM) [17], while preserving expressive power for exploration. This design enables efficient rank allocation policies that balance communication cost and model accuracy under realistic edge-cloud constraints.

In summary, compared with existing works, the key differences of this paper are three-folded: First, unlike static PEFT methods [5], [6], AirLLM realizes adaptive rank allocation by integrating wireless channel states and data characteristics. Second, compared with traditional RL [19] or regression-based refinement techniques, our hierarchical PPO-DDIM framework efficiently handles high-dimensional rank spaces and non-stationary wireless environments. Third, extensive simulation results demonstrate that we achieve a better balance between fine-tuning accuracy and communication cost, outperforming baselines in practical remote fine-tuning scenarios.

III. System Model and Problem Formulation

A. System Model

For convenience, we also list the main notations used in this paper in Table I.

1) LLM Parameter-Efficient Fine-tuning: We consider a pre-trained Transformer-based LLM $\mathscr{M}$ composed of L layers, where each layer $l \in \{1, \ldots, L\}$ contains a self-attention (SA) block and an FFN block. Without loss of generality, we exemplify the PEFT of an LLM by AdaLoRA [6]. In the SA block, AdaLoRA modules (i.e., projection matrices) are inserted into the frozen projection matrices: query ($\mathbf{W}^Q$), key ($\mathbf{W}^K$), value ($\mathbf{W}^V$), and output ($\mathbf{W}^O$). In the FFN block, AdaLoRA is similarly applied to the two linear transformations $\mathbf{W}^{\text{fc1}}$ and $\mathbf{W}^{\text{fc2}}$. During fine-tuning, the original weight matrices remain frozen, while the low-rank update matrices introduced by LoRA [5] are optimized. Mathematically, the set of LoRA-inserted modules for the l-th layer can be written as:

$$\mathcal{M}_l = \{\mathbf{W}_l^Q, \mathbf{W}_l^K, \mathbf{W}_l^V, \mathbf{W}_l^O, \mathbf{W}_l^{\text{fc1}}, \mathbf{W}_l^{\text{fc2}}\}. \tag{1}$$

TABLE I
Main notations used in this paper.

Symbol	Definition
L	Number of Transformer layers
d_h	Hidden dimension of the model
d_s	Dimension of state
d_{MLP}	Hidden size of the PPO policy multilayer perceptron (MLP)
$\mathbf{s}_t$	State at step t
$\mathbf{a}_t$	Action vector at t
$\mathbf{a}_t^{\text{out}}$	Coarse-grained action output by PPO
$\tilde{\mathbf{a}}_t$	Refined action after DDIM optimization
R_t	Reward
$\mathcal{U}(\mathbf{r}_t)$	Task loss under rank configuration
$\eta(\mathbf{r}_t)$	Communication cost of rank configuration
λ	Weighting between loss and communication cost
$\pi_\theta(\mathbf{a} \mid \mathbf{s})$	PPO policy function
$\hat{A}_t$	Advantage estimate
$J_{\text{CLIP}}(\theta)$	PPO clipped objective
$\mathcal{L}_{\text{PPO}}$	Total PPO loss
$\mathbf{x}_0$	Clean rank vector (target configuration)
$\mathbf{x}_\tau$	Noisy data at diffusion step τ
$\hat{\mathbf{x}}_0$	DDIM-predicted clean rank vector
f_ψ	Noise prediction network in DDIM
$\mathcal{L}_{\text{DDIM}}$	DDIM loss combining noise and reward terms
κ	Weighting for DDIM loss terms
T_{diff}	Number of DDIM denoising steps
$r_{\max}$	Maximum rank constraint
$\mathbf{W}_{l,m}^{(0)}$	Pre-trained weights at layer l, module m
$\mathbf{W}_{l,m}^{(t)}$	Fine-tuned weights at step t
$r_{l,m}^{(t)}$	Rank of module (l, m) at step t
$\mathscr{D}$	Fine-tuning dataset
SNR_t	Signal-to-noise ratio
W_t	Channel bandwidth
h_t	Channel gain
$\mathbf{n}_t$	AWGN noise
C_t	Channel capacity
H_t	Lexical entropy of dataset at step t
ρ_t	OOV rate of dataset at step t

Building upon AdaLoRA, we parameterize the weight update matrix using SVD [31] to support dynamic and fine-grained rank allocation. For each module m in layer l given in Eq. (1), the fine-tuned weight matrix at the t-th training step is expressed as:

$$\mathbf{W}_{l,m}^{(t)} = \mathbf{W}_{l,m}^{(0)} + \mathbf{P}_{l,m}^{(t)} \mathbf{\Lambda}_{l,m}^{(t)} \mathbf{Q}_{l,m}^{(t)}, \tag{2}$$

where $\mathbf{P}_{l,m} \in \mathbb{R}^{d_h \times r_{l,m}}$ and $\mathbf{Q}_{l,m} \in \mathbb{R}^{r_{l,m} \times d_h}$ are orthogonal matrices with the hidden dimension d_h, and the rank of the diagonal singular value matrix $\mathbf{\Lambda}_{l,m} \in \mathbb{R}^{r_{l,m} \times r_{l,m}}$ with the dimension $r_{l,m}$. In this way, the total number of trainable parameters introduced by AdaLoRA is given by $\sum_{l=1}^{L} \sum_{m \in \mathcal{M}_l} r_{l,m} (2d_h + 1)$.

To encourage the orthogonality of $\mathbf{P}_{l,m}$ and $\mathbf{Q}_{l,m}$, a *regularization term* is commonly imposed in practice, namely,

$$\mathcal{R} = \|\mathbf{P}_{l,m}{}^\top \mathbf{P}_{l,m} - \mathbf{I}\|_F^2 + \|\mathbf{Q}_{l,m} \mathbf{Q}_{l,m}{}^\top - \mathbf{I}\|_F^2, \tag{3}$$

where the Frobenius norm $\|\mathbf{A}\|_F = \sqrt{\sum_{i=1}^{m} \sum_{j=1}^{n} |a_{ij}|^2}$, of a matrix $\mathbf{A} \in \mathbb{R}^{m \times n}$ quantifies the element-wise distance between matrices [32]. This regularization ensures that $\mathbf{P}_{l,m}$ and $\mathbf{Q}_{l,m}$ approach orthogonal matrices [6].

On the other hand, the involved fine-tuning dataset $\mathcal{D} = \{D_1, D_2, \ldots, D_N\}$ can be characterized by lexical entropy and OOV rate. Specifically, for each sample $D_n \in \mathcal{D}$, the lexical entropy is defined as $H(D_n) = -\sum_{w \in \mathcal{V}} \hat{p}(w) \log \hat{p}(w)$, where $\hat{p}(w)$ is the empirical probability of word $w \in D_n$, and $\mathcal{V}$ is the vocabulary. Meanwhile, the OOV rate is calculated by $\rho(D_n) = \frac{|\{w \in D_n : w \notin \mathcal{V}\}|}{|D_n|}$, which measures the proportion of words in D that are not in the pre-defined vocabulary $\mathcal{V}$.

2) Wireless Communication Channel Model: For the remote fine-tuning of LLMs, we assume a typical cloud-edge deployment setting where the fine-tuning process is conducted on the cloud server, and the resulting low-rank parameters are transmitted to resource-constrained local edge devices. We model the wireless transmission of fine-tuned parameters from the cloud service (transmitter) to the edge device (receiver) by a slow fading Additive White Gaussian Noise (AWGN) channel [23]. Suppose each fine-tuned parameter of a module corresponding to$\mathbf{P}_{l,m}$, $\mathbf{\Lambda}_{l,m}$ and $\mathbf{Q}_{l,m}$ is first compressed and then packed into a codeword $\mathbf{c}_t \in \mathbb{C}^{b_t}$ of length b_t for transmission. The received signal at the edge is given by:

$$\mathbf{y}_t = h_t \mathbf{c}_t + \mathbf{n}_t, \tag{4}$$

where $\mathbf{y}_t$ is the received signal at the local device, h_t is the complex, slow-fading channel gain that remains constant over each block. $\mathbf{n}_t \sim \mathcal{CN}(0, \sigma_t^2 \mathbf{I}_{b_t})$ represents AWGN, with $\mathbf{I}_{b_t}$ being the b_t-dimensional identity matrix ensuring independence of noise elements. The notation $\mathcal{CN}$ denotes the complex normal distribution, where the mean is zero and the variance is σ_t^2. The average transmit power is constrained by $\frac{1}{b_t} \sum_{i=1}^{b_t} \|\mathbf{c}_t(i)\|^2 \leq P$.

Assuming perfect Channel State Information (CSI) is available at the receiver, the average achievable data rate over such a fading channel at the t-th step is:

$$C_t = \mathbb{E}_{h_t} \left[W_t \log_2 \left(1 + \text{SNR}_t \right) \right], \tag{5}$$

where W_t is the channel bandwidth while the value of SNR is calculated with $\text{SNR}_t = \frac{|h_t|^2 P}{\bar{\sigma}_t^2}$.

B. Problem Formulation

Recalling the task of transmitting fine-tuned parameters from the cloud to the edge, the number of parameters to be transmitted for each module m in layer l, as derived from Eq. (2), is $r_{l,m}^{(t)}(2d_h + 1)$. Accordingly, the transmission time can be calculated as

$$T_{l,m}^{(t)} = \frac{r_{l,m}^{(t)}(2d_h + 1) \cdot b_t}{C_t}, \tag{6}$$

where $b_t \equiv 32$ for FP32. In particular, the total transmission time is usually constrained by a maximum allowable latency $T_{\max}$, i.e.,

$$\sum\nolimits_{l=1}^{L} \sum\nolimits_{m \in \mathcal{M}_l} T_{l,m}^{(t)} \leq T_{\max}. \tag{7}$$

The constraint implicitly restricts the rank allocation across layers. Moreover, due to the limited communication capacity, there also exists a bound for the total amount of transmitted parameters, i.e., $1 \leq r_{l,m}^{(t)} \leq r_{\max}$, where $r_{\max}$ denotes the maximum allowable rank that satisfies the communication constraint.

Given these constraints on latency and rank capacity, the pivotal challenge of our scenario lies in effectively allocating ranks across modules and layers to maximize fine-tuning performance while adhering to communication budgets. Notably, since computing task-specific metrics such as accuracy at every training step is computationally expensive, the loss value $\mathcal{U}(\mathbf{r}_t)$ on the fine-tuning dataset $\mathcal{D}$ is adopted as a surrogate measure to monitor intermediate performance, thereby indirectly reflecting the model's fitness under a given rank configuration $\mathbf{r}_t = \{r_{l,m}^{(t)}\}_{l=1,m\in\mathcal{M}_l}^{L}$. Meanwhile, the associated communication cost $\eta(\mathbf{r}_t)$ is determined by the quantity of parameters transmitted from the cloud to the edge, which can be computed as:

$$\eta(\mathbf{r}_t) = \frac{\sum_{l=1}^{L} \sum_{m \in \mathcal{M}_l} r_{l,m}^{(t)}(2d_h + 1) \cdot b_t}{C_t \cdot T_{\max}}. \tag{8}$$

Mathematically, the optimization objective can be encapsulated as

$$\begin{aligned} \min_{\mathbf{r}} \quad & \mathcal{U}(\mathbf{r}_t) + \lambda \ \eta(\mathbf{r}_t) \\ \text{s.t.} \quad & \sum_{l=1}^{L} \sum_{m \in \mathcal{M}_l} \frac{r_{l,m}^{(t)}(2d_h + 1) \cdot b_t}{C_t} \leq T_{\max}, \\ & 1 \leq r_{l,m}^{(t)} \leq r_{\max}, \quad \forall l \in \{1, \ldots, L\}, \forall m \in \mathcal{M}_l, \end{aligned} \tag{9}$$

where λ is a positive weighting factor that balances the significance of model performance and communication cost. In this optimization problem, reducing the communication cost $\eta(\mathbf{r}_t)$ may lead to an increase in the loss function $\mathcal{U}(\mathbf{r}_t)$, and vice versa [21].

Conventionally, AdaLoRA allocates rank budgets $\mathbf{r}_t$ across layers based on sensitivity scores and training dynamics [6], whereas dLoRA optimizes request and adapter orchestration at serving time [24]. Neither directly incorporates dataset-dependent loss $\mathcal{U}(\mathbf{r}_t)$ and wireless communication capability C_t into fine-tuning rank allocation. Moreover, local layer-wise decisions may overlook global interactions among layers and fail to satisfy strict end-to-end constraints on parameter transmission or inference latency. Hence, identifying a meticulous design of the rank parameters for each layer that satisfies all constraints while minimizing the objective function is of utmost importance.

IV. Methodology

A. RL for Dynamic Rank Allocation

To enable dynamic rank allocation in real-world deployment scenarios, RL, particularly the PPO [19], offers a promising solution for learning adaptive policies through continuous interaction with the environment. By adopting PPO, we seek to derive a preliminary policy that effectively balances fine-tuning accuracy and communication cost under varying system conditions.

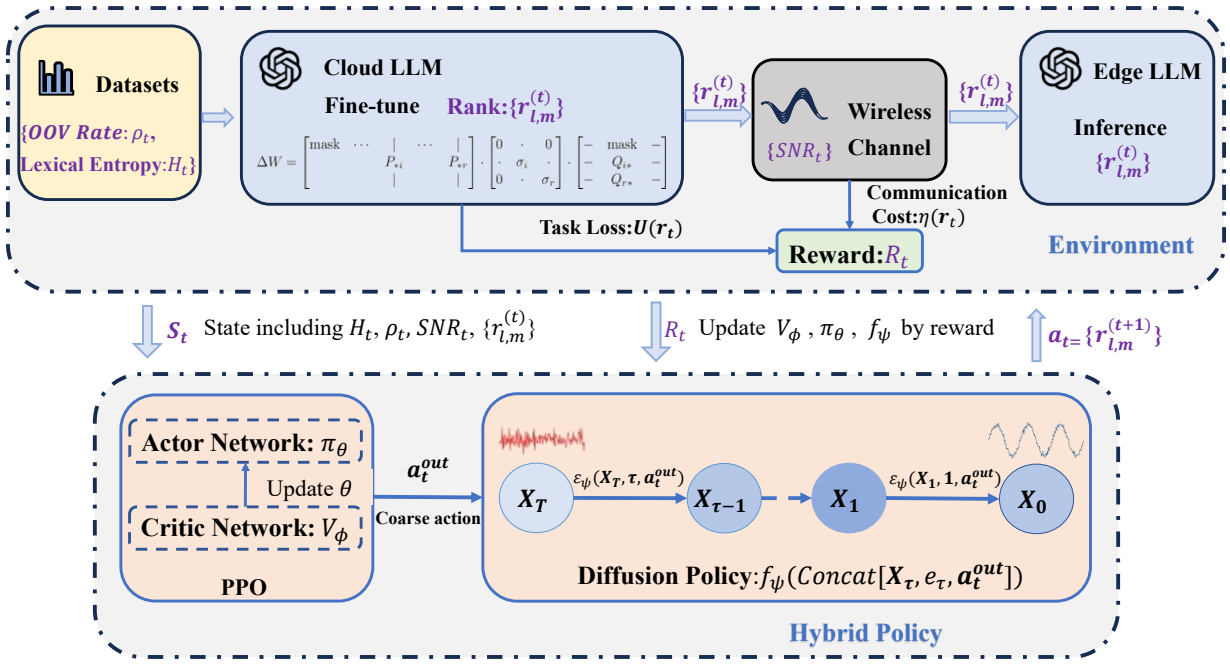

Fig. 2. Diffusion policy framework for dynamic rank allocation in remote fine-tuning.

1) MDP Formulation for Rank Allocation: RL provides a dynamically adaptive decision-making paradigm for remote fine-tuning of large models, with its core advantage lying in real-time strategy optimization through environmental feedback. To enable adaptive rank configuration under real-world constraints such as wireless bandwidth and task complexity, we formulate the rank allocation as an MDP $(\mathcal{S}, \mathcal{A}, R)$. Such assumption allows the agent to learn context-aware policies that dynamically balance compression and performance, where the action directly corresponds to the rank configuration $\mathbf{r}_t$.

- *State Representation:* The state $\mathbf{s}_t = \{\mathrm{SNR}_t, W_t, H_t, \rho_t, \mathbf{r}_t\} \in \mathcal{S}$ is designed to comprehensively capture both the system-level constraints and task-specific complexity. Correspondingly, wireless transmission capability is implicitly acquired via SNR_t and W_t through Eq. (5). Lexical entropy H_t and OOV rate ρ_t characterize the complexity of the fine-tuning dataset at time step t, reflecting how much expressive capacity (i.e., rank) the model may require and how many tokens that do not appear in the pretraining vocabulary. The current rank configuration $\mathbf{r}_t$, which represents the rank parameters for all modules in all layers, serves as the foundation upon which the next action (rank configuration) will be applied.
- *Action Space:* In our formulation, each Transformer layer contains 6 LoRA-inserted projection matrices. Thus, the action vector $\mathbf{a}_t$ at time step t (which directly defines the rank configuration) is given by $\mathbf{a}_t \in \{0, 1, \cdots, r_{\max}\}^{6L}$. And the new rank distribution $\mathbf{r}_{t+1} = \mathbf{a}_t$.
- *Reward Function:* Consistent with the objective function in Eq. (9), the reward function can be written as

$$R_t = -\mathcal{U}(\mathbf{r}_t) - \lambda \cdot \eta(\mathbf{r}_t). \tag{10}$$

where the cross-entropy loss $\mathcal{U}(\mathbf{r}_t)$ penalizes inaccurate predictions, pushing the policy to retain expressive model capacity, while normalized communication cost term $\eta(\mathbf{r}_t)$, which is proportional to the total number of transmitted parameters, encourages the policy to minimize unnecessary rank allocation. In addition, the coefficient λ controls the trade-off between accuracy and efficiency. This design allows the RL agent to learn policies that adaptively allocate ranks depending on task difficulty and system bandwidth, thereby achieving communication-efficient fine-tuning without sacrificing too much performance.

RL aims to maximize cumulative rewards through interaction with the environment. Specifically, an agent tries to learn a policy $\pi(\mathbf{a}|\mathbf{s})$, a probability distribution over actions $\mathbf{a}$ given state $\mathbf{s}$, which guides the agent's future behaviors.

2) PPO for Coarse-Grained Policy Optimization: As noted above, we adopt PPO to train a feasible policy for dynamic rank allocation. Beforehand, we briefly present the key ingredients related to PPO. In particular, the *return* at time t is defined as $\tilde{R}_t = \sum_{k=0}^{\infty} \gamma^k R_{t+k}$, where $\gamma \in (0, 1)$ discounts future rewards. The *state-value function* $V_\phi(\mathbf{s}_t) = \mathbb{E}_\pi[\tilde{R}_t|\mathbf{s}_t]$ estimates the expected return from $\mathbf{s}_t \in \mathbb{R}^{d_s}$, parameterized by a neural network with weights ϕ. The *action-value function* $Q_\pi(\mathbf{s}_t, \mathbf{a}_t) = \mathbb{E}_\pi[\tilde{R}_t|\mathbf{s}_t, \mathbf{a}_t]$ quantifies the return for action $\mathbf{a}_t$ in $\mathbf{s}_t$. The *advantage function* $\hat{A}_t = Q_\pi(\mathbf{s}_t, \mathbf{a}_t) - V_\phi(\mathbf{s}_t)$ measures how much better or worse $\mathbf{a}_t$ is compared to the average action at $\mathbf{s}_t$, thus guiding policy improvement. Since Q_π is typically unavailable, PPO estimates $\hat{A}_t$ via Generalized

Advantage Estimation (GAE) [19], using Temporal-Difference (TD) errors:

$$\hat{A}_t = \sum_{k=0}^{\infty} (\gamma\zeta)^k \delta_{t+k}, \tag{11}$$

where $\delta_t = R_t + \gamma V_{\phi_{\text{old}}}(\mathbf{s}_{t+1}) - V_{\phi_{\text{old}}}(\mathbf{s}_t)$ and $V_{\phi_{\text{old}}}(\cdot)$ denotes the value function under previous parameters for stable bootstrapping. $\zeta \in [0,1]$ is the decay factor of GAE, which controls the bias-variance trade-off in advantage estimation. Eq. (11) enables efficient estimation from sampled trajectories without computing full returns.

To stabilize policy updates of the θ-parametrized actor, PPO further introduces a clipped objective on top of the value function loss, which can be formulated as

$$\begin{aligned} J_{\text{CLIP}}(\theta) &= \min\left(r_t(\theta)\hat{A}_t, \text{clip}\left(r_t(\theta), 1-\varrho, 1+\varrho\right)\hat{A}_t\right), \\ J_V(\phi) &= \left(V_\phi(\mathbf{s}_t) - \left(\hat{A}_t + V_{\phi_{\text{old}}}(\mathbf{s}_t)\right)\right)^2, \\ \mathcal{L}_{\text{PPO}} &= \mathbb{E}\left[J_{\text{CLIP}}(\theta) + J_V(\phi)\right], \end{aligned} \tag{12}$$

where $r_t(\theta) = \pi_\theta(\mathbf{a}_t|\mathbf{s}_t)/\pi_{\theta_{\text{old}}}(\mathbf{a}_t|\mathbf{s}_t)$ is the probability ratio, measuring the likelihood of taking certain actions under the policy $\pi_\theta(\mathbf{a}_t|\mathbf{s}_t)$ versus the old one $\pi_{\theta_{\text{old}}}(\mathbf{a}_t|\mathbf{s}_t)$. $\text{clip}(r_t(\theta), 1-\varrho, 1+\varrho)$ denotes a clipping function that limits the deviation $r_t(\theta)$ between successive policy updates within the range $(1-\varrho, 1+\varrho)$. By minimizing the loss in Eq. (12) via gradient descent, we optimize both the policy π_θ and value function V_π in PPO to achieve improved decision performance. The clipped surrogate objective of PPO limits abrupt policy updates, which is desirable for coarse-grained decision-making under varying channel and task states. In the proposed hierarchical design, PPO provides coarse guidance, while the subsequent refinement stage handles the high-dimensional rank configuration.

At each decision step, the PPO agent, implemented as a two-layer multi-layer perceptron (MLP), maps the current state $\mathbf{s}_t \in \mathbb{R}^{d_s}$ to a latent action prior $\mathbf{a}_t \in \{0, 1, \ldots, r_{\max}\}^{6L}$. Given a hidden width of d_{MLP}, the computational complexity of single forward or backward pass is $\mathcal{O}\left(d_{\text{MLP}} \cdot \left(6L \cdot (r_{\max}+1) + d_s\right) + 6L \cdot (r_{\max}+1)\right)$, where the first term accounts for the two-layer MLP inference that generates logits, and the second term corresponds to the element-wise softmax computation across the discrete action heads. The complexity scales linearly with the input and output dimensions.

However, PPO's performance tends to degrade in high-dimensional discrete action spaces [19], [33]. Moreover, the gradient signal becomes increasingly sparse while the reward variations across consecutive actions remain negligible, making the estimated advantage $\hat{A}_t$ highly sensitive to noise and thereby resulting in unstable policy updates [34].

B. Diffusion Policy for High-Dimensional Actions

To mitigate the challenges of PPO in high-dimensional action space, we propose to restrict PPO to generating coarse priors $\mathbf{a}_t^{\text{out}}$ only, while delegating fine-grained decision-making $\tilde{\mathbf{a}}_t$ to a conditional diffusion model. Compared to traditional refinement techniques like Gaussian Process Regression (GPR) [35], DDIM is more appropriate for our task due to three-folded reasons: it can better capture multimodal optimal rank distributions without GPR's Gaussian assumption, scales efficiently in high dimensional spaces, and is robust to non-stationary wireless channels via iterative denoising rather than noise-sensitive one-step regression in GPR. The hierarchical coarse-to-fine strategy leverages the probabilistic noising–denoising process of diffusion models to provide a principled alternative for high-dimensional action modeling by decomposing the decision-making problem into a series of tractable local conditional distributions [16], [17]. Through the progressive denoising procedure, the hierarchical model is able to capture structural patterns across noise scales, thereby enhancing exploration capabilities and improving robustness when combined with PPO [16]. The detailed procedure is illustrated in Fig. 2.

Algorithm 1 The Training of Hierarchical PPO-DDIM Adaptive Rank Allocation Policy.

Input: Initialized model and hyper-parameters.
Output: Trained hierarchical policy (π_θ, f_ψ) for adaptive rank allocation.

for episode = $1, 2, \ldots,$ **do**
  Observe initial state $\mathbf{s}_0$;
  for step $t = \{1, \ldots, T_{\text{env}}\}$ **do**
    Generate coarse action $\mathbf{a}_t^{out} \sim \pi_{\theta_{\text{old}}}(\cdot|\mathbf{s}_t)$;
    // PPO outputs low-dimensional guidance
    Initialize noise latent $\mathbf{x}_{T_{\text{diff}}} \sim \mathcal{N}(\mathbf{0}, \mathbf{I})$;
    for $\tau = \{T_{\text{diff}} - 1, \ldots, 0\}$ **do**
      Obtain the conditional noise prediction $\tilde{\boldsymbol{\epsilon}}_{\tau,\psi}$ with Eq. (15)
      // DDIM refines via a_t^{out} conditioning
      Predict the clean sample $\hat{\mathbf{x}}_0$ with Eq. (16);
      Refine action using DDIM procedure with Eq. (17);
    end for
    Decode refined action through Eq. (18);
    Deploy the rank configuration to obtain the next state $\mathbf{s}_{t+1}$;
    Compute reward using Eq. (10) and collect transition $\{\mathbf{s}_t, \tilde{\mathbf{a}}_t, R_t, \mathbf{s}_{t+1}\}$ into batch $\mathcal{B}$;
  end for
  Compute PPO loss using samples from $\mathcal{B}$ with Eq. (12);
  Update PPO policy π_θ and value function V_π;
  for $\tau = \{0, \ldots, T\}$ **do**
    Generate noisy sample $\mathbf{x}_\tau$ from clean input $\mathbf{x}_0$ using Eq. (13);
    Compute the hybrid loss according to Eq. (19);
    Update the parameters in noise network f_ψ via the gradient descent.
  end for
end for

1) Conditional Diffusion Refinement Guided by PPO Priors: We begin by briefly introducing the forward and reverse processes of the DDPM and its deterministic variant DDIM, which achieves faster inference with similar generative quality

[18]. Notably, DDIM shares the same training objective and noise schedule as DDPM, with the main distinction residing in the sampling procedure used during inference.

a) Forward Diffusion Process.: To enable diffusion-based training, it is essential to apply a forward noise injection process to the training data. Specifically, each clean rank configuration vector $\mathbf{x}_0$ is progressively corrupted by injecting Gaussian noise over T discrete steps. Formally, at each timestep $\tau \in \{1, \ldots, T\}$, the conditional distribution of the noisy latent variable $\mathbf{x}_\tau$ given the previous state $\mathbf{x}_{\tau-1}$ is defined as

$$q(\mathbf{x}_\tau|\mathbf{x}_{\tau-1}) = \mathcal{N}\left(\mathbf{x}_\tau; \sqrt{\alpha_\tau}\mathbf{x}_{\tau-1}, (1-\alpha_\tau)\mathbf{I}\right), \tag{13}$$

where the noise schedule parameters $\alpha_\tau \in (0,1)$ control the amount of noise injected, and $\mathcal{N}(\cdot; \boldsymbol{\mu}, \boldsymbol{\Sigma})$ denotes a Gaussian distribution with mean $\boldsymbol{\mu}$ and covariance $\boldsymbol{\Sigma}$. By marginalizing over intermediate variables, the closed-form distribution of $\mathbf{x}_\tau$ conditioned on the clean sample $\mathbf{x}_0$ is given by

$$q(\mathbf{x}_\tau|\mathbf{x}_0) = \mathcal{N}\left(\mathbf{x}_\tau; \sqrt{\bar{\alpha}_\tau}\mathbf{x}_0, (1-\bar{\alpha}_\tau)\mathbf{I}\right). \tag{14}$$

Here, $\bar{\alpha}_\tau = \prod_{s=1}^{\tau} \alpha_s = \prod_{s=1}^{t}(1-\beta_s)$ represents the cumulative product of the noise schedule up to timestep τ.

b) Conditional Reverse Denoising Process.: The reverse diffusion process aims to iteratively denoise $\mathbf{x}_\tau$ back to the clean signal estimate $\mathbf{x}_0$. Serving as a critical component of the inference procedure, the denoising step is parameterized by a neural network $f_\psi(\cdot)$ that predicts the injected noise at each step. To incorporate guidance from the PPO output $\mathbf{a}_t^{\text{out}}$, the noise estimator is conditioned on both the noisy latent and the PPO output $\mathbf{a}_t^{\text{out}}$, together with the timestep embedding $\mathbf{e}_\tau$ that encodes the current diffusion step. Mathematically, the obtained conditional noise prediction, denoting as $\tilde{\boldsymbol{\epsilon}}_{\tau,\psi}$, can be encapsulated as

$$\tilde{\boldsymbol{\epsilon}}_{\tau,\psi} = f_\psi\left(\text{Concat}[\mathbf{x}_\tau, \mathbf{e}_\tau, \mathbf{a}_t^{\text{out}}]\right), \tag{15}$$

where $\mathbf{e}_\tau$ is typically implemented as a sinusoidal positional encoding to provide temporal context, and $f_\psi(\cdot)$ denotes the denoising network, which can be realized as a U-Net architecture [36] or a residual MLP depending on model scale and complexity.

Using the predicted noise, the posterior mean estimator of the clean signal at timestep τ is computed as

$$\mu_\psi(\mathbf{x}_\tau, \tau, \mathbf{a}_t^{\text{out}}) = \frac{1}{\sqrt{\alpha_\tau}}\left(\mathbf{x}_\tau - \frac{1-\alpha_\tau}{\sqrt{1-\bar{\alpha}_\tau}}\tilde{\boldsymbol{\epsilon}}_{\tau,\psi}\right). \tag{16}$$

Following the standard DDPM posterior mean, the expression can incorporate the PPO prior as a conditioning signal and generate a fine-tuned $\tilde{\mathbf{a}}_t$ for the rank allocation task.

c) Deterministic Sampling via DDIM.: For inference, we employ the DDIM sampler, which enables deterministic and efficient reconstruction of the clean action vector. Starting from an initial latent $\mathbf{x}_T \sim \mathcal{N}(0, \mathbf{I})$, the reverse trajectory is computed recursively, where at each step $\tau - 1$, the latent vector $\mathbf{x}_{\tau-1}$ is estimated from the current value $\mathbf{x}_\tau$ as

$$\mathbf{x}_{\tau-1} = \sqrt{\bar{\alpha}_{\tau-1}}\hat{\mathbf{x}}_0 + \sqrt{1-\bar{\alpha}_{\tau-1}-\sigma_\tau^2}\tilde{\boldsymbol{\epsilon}}_{\tau,\psi} + \sigma_\tau\boldsymbol{\epsilon}, \tag{17}$$

where $\hat{\mathbf{x}}_0 := \mu_\psi(\mathbf{x}_\tau, \tau, \mathbf{a}_t^{\text{out}})$ is the predicted clean sample, $\boldsymbol{\epsilon} \sim \mathcal{N}(0, \mathbf{I})$ is an additional noise term, and $\sigma_\tau \geq 0$ controls the stochasticity of the sampler with $\sigma_\tau = 0$ yielding fully deterministic DDIM sampling.

After completing $T_{\text{diff}} \leq T$ reverse steps, the final latent $\mathbf{x}_0$ is transformed into the actionable discrete vector by rounding and clipping, which is formulated by

$$\tilde{\mathbf{a}}_t = \text{clip}\left(\lfloor \mathbf{x}_0 \rfloor, 0, r_{\max}\right), \tag{18}$$

where $r_{\max}$ denotes the maximum allowed rank value per dimension, ensuring validity and executability of the generated action. $\lfloor \cdot \rfloor$ represents element-wise flooring to the nearest lower integer.

2) Hybrid Training Objective and Optimization.: To enhance controllability without relying on external classifiers, the training adopts the CFG strategy [37]. Specifically, the conditional diffusion model is trained to minimize a hybrid loss that combines reconstruction fidelity in noise prediction and policy effectiveness measured via task reward,

$$\mathcal{L}_{\text{DDIM}} = \mathbb{E}_{\mathbf{x}_0,\tau,\boldsymbol{\epsilon},\mathbf{a}_t^{\text{out}}}\left[\|\tilde{\boldsymbol{\epsilon}}_{\tau,\psi} - \boldsymbol{\epsilon}\|_2^2\right] - \kappa \cdot \mathbb{E}_{\mathbf{s}_t,\tilde{\mathbf{a}}_t}[R_t], \tag{19}$$

where the noise $\boldsymbol{\epsilon} \sim \mathcal{N}(0, \mathbf{I})$ is the ground-truth noise added at timestep τ, R_t is the reward obtained from executing the refined action $\tilde{\mathbf{a}}_t$ in state $\mathbf{s}_t$ as defined in Eq. (10), and $\kappa > 0$ is a hyperparameter balancing denoising accuracy and policy reward maximization.

To maintain stability and promote complementary learning between the coarse and fine policies, we adopt an alternating training strategy that iteratively updates PPO and DDIM with shared trajectory data. Algorithm 1 summarizes the entire inference and training process for reference.

Notably, the inference follows a clear two-stage design that tightly couples PPO and DDIM. Fist, PPO observes the wireless channel state (including SNR and bandwidth) and the linguistic complexity of the dataset, then outputs a low-dimensional coarse-grained guidance vector $\mathbf{a}_t^{out}$. This vector captures the overall trade-off between fine-tuning accuracy and communication cost, providing stable high-level guidance for rank allocation. Based on this conditional guidance, DDIM further explores the structural dependencies among Transformer layers, and expands the coarse guidance into a complete high-dimensional, layer-specific rank configuration $\tilde{\mathbf{a}}_t$. In this way, PPO focuses on global decision-making, while DDIM performs a fine-grained optimization to maintain model performance.

To ensure stable and effective training, we adopt an alternating training strategy. In the PPO update stage, we fix the DDIM module and use the obtained reward R_t to update the PPO policy via the clipped surrogate loss (Eq. (12)), so that PPO gradually learns better coarse-grained guidance strategies. In the DDIM update stage, we fix the PPO module and use high-quality trajectories from the replay buffer to train DDIM. DDIM learns to map the coarse guidance to high-performance rank configurations by minimizing the hybrid loss function (Eq. (19)). Such alternating optimization ensures that both components reinforce each other and steadily improve the overall performance.

3) Computational Complexity Analyses: To circumvent the severe inefficiency of vanilla PPO in high-dimensional discrete action spaces, we reformulate the policy as a low-dimensional continuous vector generator and discard the costly softmax operation, cutting down redundant complexity by $\mathcal{O}(6L \cdot (r_{\max}+1))$. Different from vanilla PPO suffering from exponential complexity in the $6L$-dimensional discrete action space, our revised lightweight PPO outputs only a compact low-dimensional latent vector $\mathbf{a}_t^{\text{out}}$. Assuming the dimension of this coarse latent representation is $D_{\text{low}} \ll 6L$, the computational complexity of our modified PPO policy network scales as $\mathcal{O}(D_{\text{low}}^2)$, which is negligible and nearly constant with respect to the full $6L$ space. Notably, we decompose the decision-making process into two complementary stages: coarse-grained PPO guidance and fine-grained DDIM refinement. The coarse-grained output $\mathbf{a}_t^{\text{out}}$ produced by PPO has a tiny dimension, far smaller than that of the final $6L$-dimensional discrete rank vector $\mathbf{a}_t \in \mathbb{Z}^{6L}$. Such dimensional decoupling is the core of our complexity optimization and effectively eliminates the curse of dimensionality.

The fine-grained action optimization is completed by a conditional DDIM module, which takes the coarse latent $\mathbf{a}_t^{\text{out}}$ as conditional guidance, and refines a randomly initialized Gaussian latent $\mathbf{x}_T \sim \mathcal{N}(0, \mathbf{I})$ into a reasonable structured rank vector. For DDIM equipped with a two-residual-block MLP denoiser with hidden width d_{latent}, its per-step denoising complexity scales linearly with $6L$ and d_{latent}. Given that T_{diff} (diffusion steps) is set to a small fixed constant, the total inference complexity of DDIM is $\mathcal{O}(T_{\text{diff}} \cdot L \cdot d_{\text{latent}})$, keeping efficient and tractable even for large-scale Transformer models with huge L. When the more powerful U-Net is adopted as the denoiser, the per-step complexity is $\mathcal{O}\left(C_{\text{in}}^2 \cdot L_s \cdot 2^{L_{\text{depth}}}\right)$ where C_{in} denotes the input channel dimension of U-Net, $L_s = 6L$ represents the dimension of the rank action space, and L_{depth} is the network depth of U-Net. After T_{diff} denoising steps, the total inference cost turns to $\mathcal{O}\left(T_{\text{diff}} \cdot C_{\text{in}}^2 \cdot L_s \cdot 2^{L_{\text{depth}}}\right)$. This cost still follows linear scaling with L_s and avoids exponential growth, remaining feasible for deployment.

In a nutshell, the total inference complexity of the hybrid PPO-DDIM framework sums the overhead of the low-dimensional PPO branch and the diffusion refinement branch. The modified PPO introduces only negligible $\mathcal{O}(D_{\text{low}}^2)$ computational overhead, while the DDIM component scales linearly with the target high-dimensional action size $6L$. This hybrid design thoroughly avoids the exponential complexity of vanilla PPO in high-dimensional spaces, guaranteeing efficient and stable inference for large-scale LLM low-rank adaptation.

V. Experimental Results

A. Experimental Settings

This section presents comprehensive experimental results designed to validate the effectiveness of AirLLM for remote fine-tuning of LLMs. All experiments use the SST-2 dataset [38] (i.e., a binary classification dataset for sentiment analysis, consisting of $67,349$ training samples and 872 test samples, where each sample is a sentence labeled as positive or negative sentiment). We adopt the OPT-1.3B model [39], a decoder-only Transformer model with 24 layers, 12 attention heads per layer, a hidden dimension of $2,048$, and a total of 1.3 billion parameters; this model is equipped with LoRA adapters for all linear projection layers (including attention query, key, value, and output layers) with a default rank of $r = 8$ to enable parameter-efficient fine-tuning. For LLM fine-tuning, we use a batch size of 32, weight decay of 10^{-5}, and AdamW optimizer with $\beta_1 = 0.9$ and $\beta_2 = 0.999$. Hyperparameters for PPO training and the diffusion policy (e.g., learning rates, diffusion steps) are fully provided in Table II. Wireless communication is modeled as an AWGN channel with 100 MHz bandwidth, 1s latency, and SNR levels ranging from -5 dB to 15 dB. The total number of training steps is set to $15,000$ and we evaluate accuracy every 100 step during the training process. If the reward value exceeds $\min[-\lambda, -0.5]$ and the accuracy does not improve for 5 consecutive evaluations, we terminate training, and such an *early stopping* strategy applies for all models to ensure consistency [40]. Notably, this choice of reward convergence threshold is motivated by the following observation: when λ is very small (e.g., $\lambda = 0.1$ or 0.01), the second term in Eq. (10) has a slight influence on the overall reward, and a reward value of -0.5 is considered sufficient to indicate convergence. In contrast, when λ is larger (e.g., $\lambda = 1$), the second term becomes more dominant, and the overall reward is lower. In this case, we consider $-\lambda$ as a sufficiently high reward value. We compare AirLLM against AdaLoRA [6] and random rank allocation baselines, where AdaLoRA is a state-of-the-art parameter-efficient fine-tuning method that adaptively allocates low-rank budgets across layers and modules (with the same LoRA rank $r = 8$ as AirLLM for fair comparison), and Random Rank Allocation is a naive baseline that randomly assigns ranks to each LoRA adapter without adaptive optimization. And we evaluate the performance in terms of binary classification accuracy. Finally, we summarize the default parameter settings in Table II.

TABLE II
Default parameter settings in simulations.

Parameter	**Value**
MLP hidden size (d_{MLP})	256
Discount factor (γ)	0.95
Decay factor of GAE (ζ)	0.95
U-Net depth (D)	6
Kernel size (k)	3
Batch size	32
Learning rate of PPO	1×10^{-4}
Learning rate of DDIM	5×10^{-5}
Random seeds	42
Hybrid loss weight (κ)	0.1
Reward balance factor (λ)	0.01, 0.1, 1
Total training steps	$15,000$
DDIM inference steps (T_{diff})	30, 50, 100
DDPM Training steps	600, 800, $1,000$
PPO clipping factor (ϱ)	0.2
Evaluating steps	100
Maximum rank constraint ($r_{\max}$)	8, 16, 32, 64, 128
SNR (dB)	-5, 0, 5, 10, 15
DDIM prediction strategy	$\boldsymbol{v}$-, $\boldsymbol{\epsilon}$-, $\boldsymbol{x_0}$-prediction
Noise schedule (β)	linear, cosine, scaled-linear

B. Simulation Results

TABLE III
PERFORMANCE COMPARISON IN TERMS OF PREDICTION ACCURACY.

Metric	AirLLM					AdaLoRA
	PPO	DDIM	PPO+DDPM	PPO+DDIM/MLP	PPO+DDIM/U-Net	
Accuracy	94.50%	94.72%	95.41%	95.53%	95.30%	95.18%
Communication Cost	0.862	0.858	0.821	**0.795**	0.808	0.843
Convergence Steps	12500	8800	9200	**7800**	8500	8000
Inference Latency (ms)	0.95	1.02	1.28	**1.10**	5.35	0.88

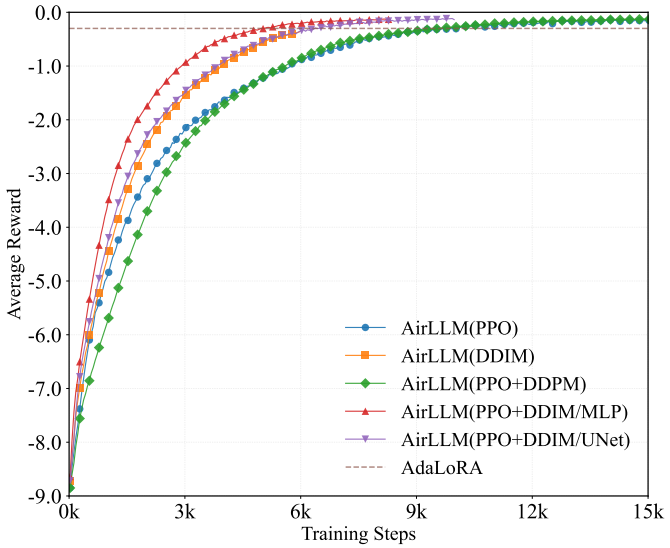

Fig. 3. Comparison of average reward for different training methods.

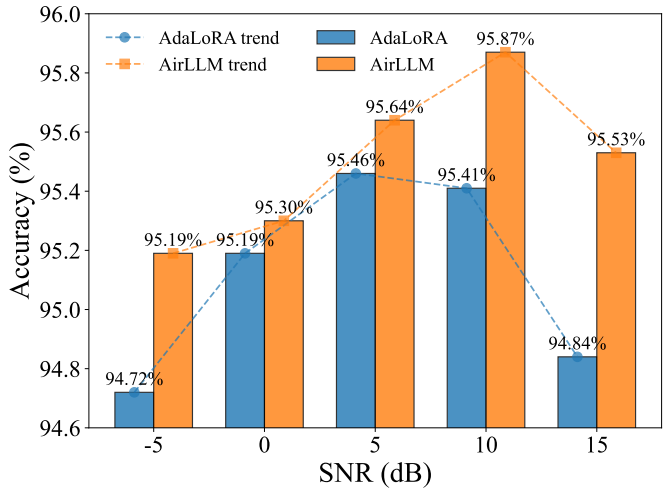

Fig. 4. Accuracy performance evaluated under diverse SNRs.

1) Performance Comparison: Table III comprehensively compares the proposed AirLLM (with different variants) with AdaLoRA, covering not only prediction accuracy but also communication cost, convergence speed, and inference latency—key metrics to evaluate the balance between performance and efficiency. Several variants of AirLLM with different RL algorithms are leveraged, and we also study the performance differences when using MLP and U-Net as backbones of DDIM. On the other hand, Fig. 3 gives the corresponding convergence curves. It can be observed from Table III and Fig. 3 that standalone PPO or DDIM yield the lowest accuracy, higher communication cost, slower convergence, and less efficient inference. Specifically, standalone PPO and DDIM exhibit notably higher communication overhead and slower convergence compared to integrated AirLLM variants, while their inference efficiency, though relatively competitive in some cases, comes at the cost of significantly compromised accuracy. This confirms the inefficiency of single-module designs in balancing performance and deployment efficiency. Instead, regardless of the backbone of either MLP or U-Net, the hierarchical integration achieves superior performance in all metrics. Meanwhile, the integration of PPO with DDIM accelerates the convergence compared to that with DDPM, reduces communication overhead, and maintains moderate inference latency. Compared to PPO+DDPM, the PPO+DDIM combination shows clear advantages in convergence speed and communication efficiency, while keeping inference latency at a manageable level that meets the requirements of remote fine-tuning scenarios. Finally, alongside its computational efficiency, the use of MLP also leads to better results, as shown by its lower inference latency and higher accuracy compared to U-Net-based variants in Table III. Notably, MLP-based AirLLM variants maintain efficient inference latency that is comparable to baseline methods, while U-Net-based variants suffer from significantly higher latency due to their more complex network structure.

Although AirLLM(PPO) and AirLLM(PPO+DDIM/MLP) achieve similar final rewards (i.e., a composition of task loss and communication cost) in Fig. 3, since the task loss is not strictly proportional to classification accuracy, the more expressive diffusion model can better explore the rank space and discover more favorable LoRA rank assignments, leading to higher accuracy in Table III.

As shown in Table III, AirLLM (PPO+DDIM/MLP) achieves 95.53% accuracy, which is higher than the state-of-the-art baseline AdaLoRA (95.18%). Meanwhile, our method obtains a lower communication cost of 0.795 compared with 0.843 for AdaLoRA, and converges much faster with only $7,800$ steps. The results confirm that AirLLM can achieve better accuracy with lower communication overhead and higher efficiency than AdaLoRA, making it more suitable for wireless remote fine-tuning.

In addition to efficiency and convergence speed, as shown in Fig. 4, AirLLM demonstrates superior robustness under varying channel conditions. Specifically, AirLLM achieves 0.11-0.69 percentage points higher accuracy compared to AdaLoRA, consistently adapting its rank configurations under

TABLE IV
COMPARISON IN TERMS OF ACCURACY AND TRANSMITTED PARAMETERS.

Rank ($r_{\max}$)	Accuracy (%)		Transmitted Parameters	
	AdaLoRA	AirLLM	AdaLoRA	AirLLM
8	95.18	**95.64** ↑	4,718,592	4,235,648 ↓
16	94.72	**95.30** ↑	9,437,184	8,471,296 ↓
32	95.41	**95.87** ↑	18,874,368	16,942,592 ↓
64	94.84	**95.53** ↑	32,399,048	28,234,160 ↓
128	94.72	**95.19** ↑	63,870,464	56,664,832 ↓

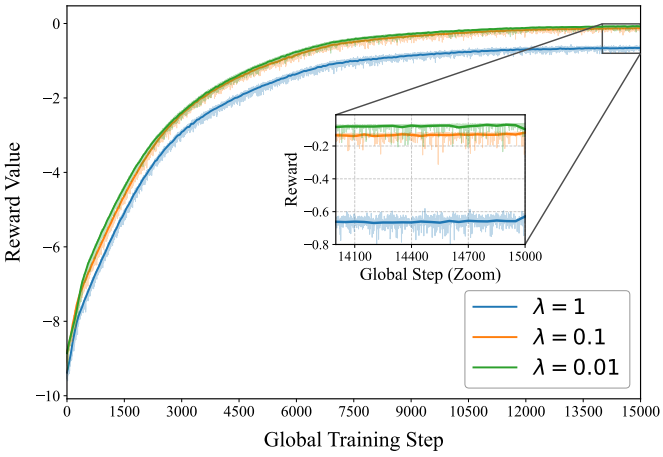

Fig. 5. Impact of reward coefficient λ.

varying wireless channel conditions. Notably, the accuracy exhibits moderate fluctuations across different SNR conditions rather than a strictly monotonic trend. This is because AirLLM jointly optimizes task loss and communication cost rather than classification accuracy alone, and different SNR conditions may therefore lead to different rank configurations. Furthermore, benchmarking experiments in Table IV comprehensively evaluate AirLLM against AdaLoRA under varying rank budgets (i.e., $r_{\max}$). The results demonstrate that AirLLM consistently outperforms the baseline across all settings. Particularly, it achieves a notable higher accuracy at $r_{\max} = 64$ while simultaneously reducing transmitted parameters by 12.5%. These results collectively validate the effectiveness of AirLLM: by unifying PPO's stability and DDIM's high-dimensional modeling, the framework meets the dual objectives of high accuracy and communication efficiency in remote fine-tuning scenarios, confirming the theoretical motivation proposed in Section IV.

These results collectively validate that AirLLM achieves a superior balance between classification accuracy, communication overhead, convergence efficiency, and inference complexity, which is critical for communication-constrained remote LLM fine-tuning.

2) Performance Sensitivity Studies: Next, we examine the impact of the reward balancing coefficient λ, which as defined in Eq. (10), regulates the trade-off between task accuracy and communication cost. Fig. 5 shows $\lambda = 0.1$ or $\lambda = 0.01$ achieves superior, competitive balance, namely higher reward values with faster convergence. Table V(a) further confirms

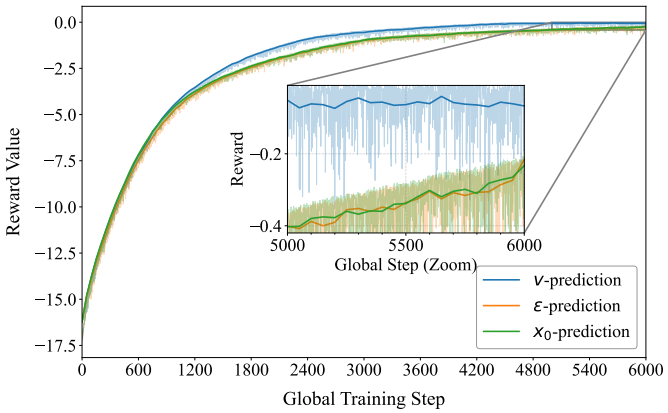

Fig. 6. The training reward of policy with different DDIM prediction strategies.

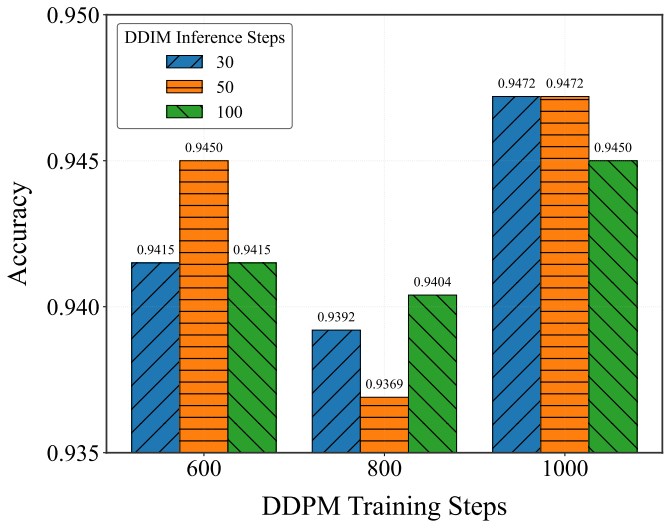

Fig. 7. Accuracy performance evaluated under varying DDPM training steps and DDIM Inference steps.

the superiority of $\lambda = 0.1$ in classification accuracy. On the contrary, a smaller λ compromises the balance.

We further consider different DDIM prediction strategies [30], each representing a distinct modeling choice. The $\boldsymbol{\epsilon}$-prediction estimates residual noise, directly aligning with the probabilistic structure of the diffusion process for stable and accurate reconstruction. The $\boldsymbol{v}$-prediction models a velocity-like intermediate variable defined as $\boldsymbol{v} = \sqrt{\bar{\alpha}_t}\,\boldsymbol{\epsilon} - \sqrt{1-\bar{\alpha}_t}\,\boldsymbol{x}_0$, which combines both noise and clean signal components, offering a balanced view of the denoising dynamics. The $\boldsymbol{x_0}$-

TABLE V
CLASSIFICATION ACCURACY UNDER DIFFERENT SETTINGS.

(a) Accuracy for Different λ Values			
	$\lambda = 1$	$\lambda = 0.1$	$\lambda = 0.01$
Accuracy	95.07%	95.41%	94.95%
(b) Accuracy for Different Prediction Types			
	v-prediction	**ϵ-prediction**	**x_0-prediction**
Accuracy	95.30%	95.30%	95.07%

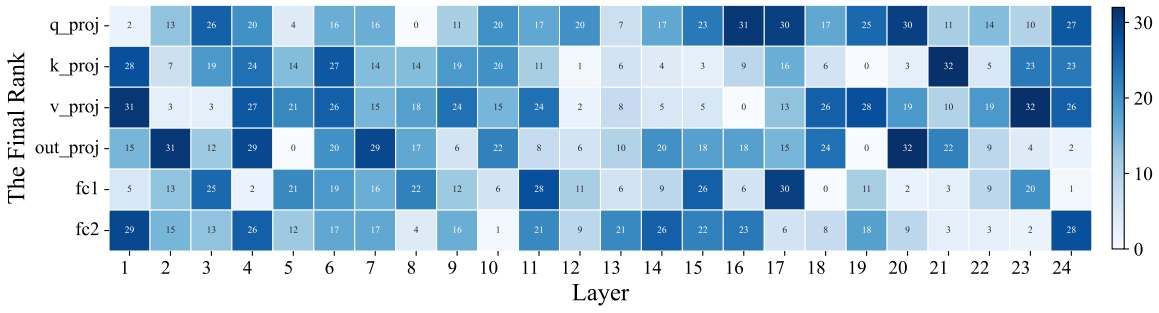

(a) cos

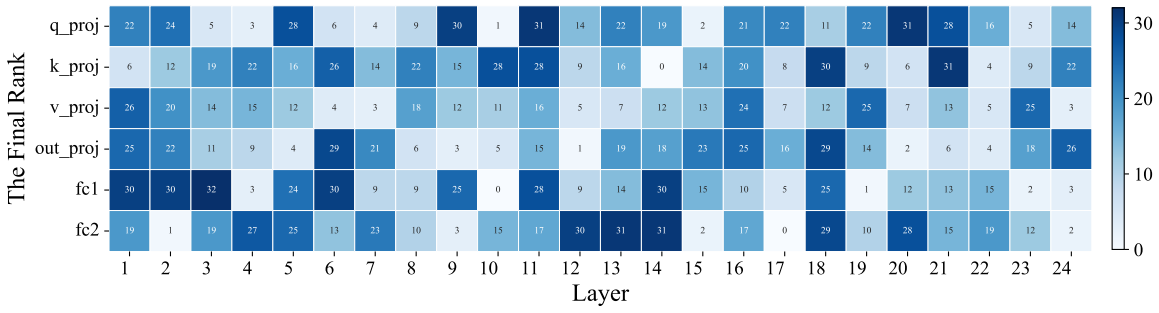

(b) linear

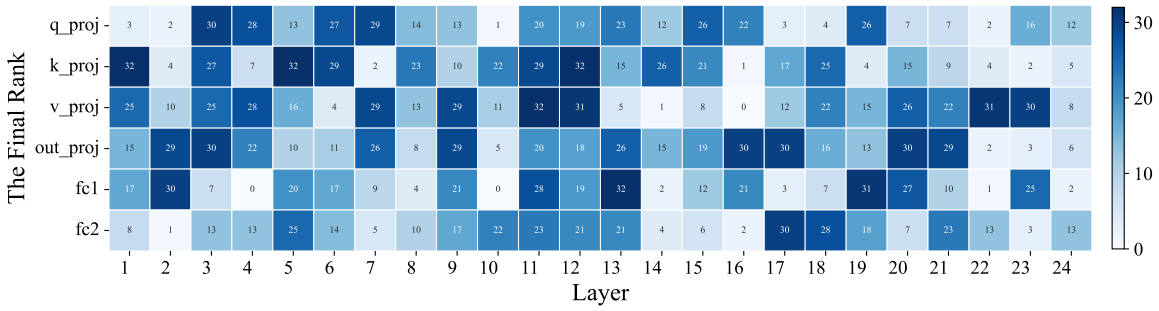

(c) scaled_linear

Fig. 8. Rank distribution under different β schedules.

prediction directly targets the clean data, but this approach is more sensitive to boundary effects in high-dimensional spaces, leading to larger convergence fluctuations. Table V(b) shows that both $\boldsymbol{\epsilon}$-prediction and $\boldsymbol{v}$-prediction achieve high accuracy, outperforming $\boldsymbol{x_0}$-prediction at a lower value. Similarly, Fig 6 shows $\boldsymbol{v}$-prediction obtain higher reward, however, the other two prediction methods also gain a high reward. These results further confirm the advantage of residual noise or intermediate variable modeling over direct data recovery for dynamic rank allocation in diffusion-based policies.

Fig. 7 presents the impact of different training and inference steps. It can be observed that the configuration with $1,000$ steps for training and 50 steps for inference achieves 95.30% accuracy. As shown in Table VI, under the same number of DDPM training steps, we set different DDIM inference steps to complete the full training of $1,000$ episodes. The comparison indicates that the training time increases significantly as the number of inference steps grows, demonstrating a direct impact of inference steps on the overall training duration. For DDIM inference steps (T_{diff}), increasing the inference steps from 30 to 100 raises the total time by over 20% while bringing only marginal accuracy improvement. Sufficient training enables the diffusion model to learn noise patterns, while excessive inference steps ($T_{\text{diff}} \geq 50$) increase latency by 40% with negligible gains.

TABLE VI
TOTAL INFERENCE TIME (S) FOR DIFFERENT INFERENCE STEPS.

DDPM Training Steps	DDIM Inference Steps	Total Time (s)
600	30	907
600	50	$1,037$
600	100	$1,101$

In addition, we provide comprehensive sensitivity analysis

on noise schedule parameters (β), which govern the diffusion trajectory and final rank allocation behavior. The β schedule in Eq. (16) shapes the rank distribution by controlling noise degradation. Fig. 8 shows that the scaled-linear schedule outperforms alternatives and assigns higher average ranks to lower layers. For the evaluated OPT-1.3B model, this allocation pattern indicates a greater contribution from lower-layer modules under the selected objective. In addition, the schedule allocates larger ranks to critical modules such as $\mathbf{W}^O$ and $\mathbf{W}^{\text{fc1}}$, aligning with the findings of AdaLoRA [6] on the importance of these components for preserving task performance. This matches the cumulative SNR expression $\bar{\alpha}_t = \prod(1-\beta_s)$, where slower noise degradation in lower layers preserves essential rank information, while faster degradation in higher layers effectively prunes redundant parameters, thereby improving communication efficiency for OPT-1.3B.

VI. Conclusion

This paper has presented AirLLM, a novel framework for communication-efficient remote fine-tuning of LLMs. Compared to the static rank allocation in AdaLoRA, AirLLM has integrated PPO with DDIM to dynamically optimize allocated ranks, further affecting the fine-tuned SVD matrices for over-the-air transmission. The PPO and DDIM components are alternately trained in a decoupled manner, where DDIM adopts the CFG strategy to improve controllability and reward alignment. By embedding channel conditions (SNR and bandwidth) and dataset characteristics (lexical entropy and out-of-vocabulary rate) into an RL state space, AirLLM has adaptively balanced model performance and parameter transmission efficiency. Particularly, AirLLM has achieved up to a 0.69% accuracy improvement over AdaLoRA while reducing transmitted parameters by 12.5% at $r_{\max} = 64$. The convergence speed has been accelerated by 20–30% via DDIM sampling, showcasing the framework's effectiveness in high-dimensional action spaces. These findings have validated AirLLM's superior efficiency in remote fine-tuning of LLMs. Future work may explore multi-agent collaboration and adaptive noise scheduling to enhance scalability and robustness in extreme channel conditions.

References

[1] OpenAI, "GPT-4 technical report," OpenAI, Tech. Rep. arXiv:2303.08774, 2023, arXiv preprint arXiv:2303.08774. [Online]. Available: https://arxiv.org/abs/2303.08774

[2] DeepSeek-AI, "Deepseek-v2 technical report," DeepSeek-AI, Tech. Rep. arXiv:2405.04434, 2024, arXiv preprint arXiv:2405.04434. [Online]. Available: https://arxiv.org/abs/2405.04434

[3] W. X. Zhao, K. Zhou, J. Li, T. Tang, X. Wang, Y. Hou, Y. Min, B. Zhang, J. Zhang, Z. Dong, Y. Du, C. Yang, Y. Chen, Z. Chen, J. Jiang, R. Ren, Y. Li, X. Tang, Z. Liu, P. Liu, J.-Y. Nie, and J.-R. Wen, "A survey of large language models," *arXiv preprint arXiv:2303.18223*, 2023. [Online]. Available: https://arxiv.org/abs/2303.18223

[4] V. Lialin, V. Deshpande, and A. Rumshisky, "Scaling down to scale up: A guide to parameter-efficient fine-tuning," *arXiv preprint arXiv:2303.15647*, 2023.

[5] E. J. Hu, Y. Shen, P. Wallis, Z. Allen-Zhu, Y. Li, S. Wang, L. Wang, and W. Chen, "LoRA: Low-Rank adaptation of large language models," in *Proc. ICLR*, Virtual Edition, Apr. 2022.

[6] Q. Zhang, Z. Liu, J. Fu, H. Dong, X. Han, P. Zhang, Y. Sun, H. Tian, H. Wu, and H. Wang, "AdaLoRA: Adaptive budget allocation for parameter-efficient fine-tuning," in *Proc. ICLR*, Kigali, Rwanda, May 2023.

[7] A. R. Hummaida, N. W. Paton, and R. Sakellariou, "Adaptation in cloud resource configuration: a survey," *J. Cloud Comput.*, vol. 5, no. 1, p. 7, 2016.

[8] B. Xu, L. Zhang, Z. Mao, Q. Wang, H. Xie, and Y. Zhang, "Curriculum learning for natural language understanding," in *Proc. ACL*, Virtual Edition, Jul. 2020.

[9] S. Han, H. Mao, and W. J. Dally, "Deep compression: Compressing deep neural networks with pruning, trained quantization and huffman coding," in *Proc. ICLR*, San Juan, Puerto Rico, May 2016.

[10] X. Qiu, T. Sun, Y. Xu, Y. Shao, N. Dai, and X. Huang, "Pre-trained models for natural language processing: A survey," *Sci. China Technol. Sci.*, vol. 63, no. 10, pp. 1872–1897, 2020.

[11] H. Yang, P. F. Smulders, and M. H. Herben, "Channel characteristics and transmission performance for various channel configurations at 60 GHz," *Eurasip J. Wirel. Commun. Netw.*, vol. 2007, no. 1, p. 019613, 2007.

[12] G. Bebis and M. Georgiopoulos, "Feed-forward neural networks," *IEEE Potentials*, vol. 13, no. 4, pp. 27–31, 1994.

[13] C. U. Bas, R. Wang, S. Sangodoyin, D. Psychoudakis, T. Henige, R. Monroe, J. Park, C. J. Zhang, and A. F. Molisch, "Real-time millimeter-wave MIMO channel sounder for dynamic directional measurements," *IEEE Trans. Veh. Technol.*, vol. 68, no. 9, pp. 8775–8789, 2019.

[14] C. Szepesvári, *Algorithms for reinforcement learning*. Morgan & Claypool Publishers, 2010.

[15] Z. Qi, Y. Feng, and Z. Qin, "Adaptive sampling and joint semantic-channel coding under dynamic channel environment," *arXiv preprint arXiv:2502.07236*, 2025.

[16] A. Z. Ren, J. Lidard, L. L. Ankile, A. Simeonov, P. Agrawal, A. Majumdar, B. Burchfiel, H. Dai, and M. Simchowitz, "Diffusion policy policy optimization," in *Proc. ICLR*, Singapore, Apr 2025.

[17] J. Ho, A. Jain, and P. Abbeel, "Denoising diffusion probabilistic models," in *Proc. NeurIPS*, Virtual Edition, Dec. 2020.

[18] J. Song, C. Meng, and S. Ermon, "Denoising diffusion implicit models," in *Proc. ICLR*, Vienna, Austria, May 2021.

[19] J. Schulman, F. Wolski, P. Dhariwal, A. Radford, and O. Klimov, "Proximal policy optimization algorithms," *arXiv preprint arXiv:1707.06347*, 2017.

[20] C. Clarke, Y. Heng, L. Tang, and J. Mars, "PEFT-U: Parameter-efficient fine-tuning for user personalization," *arXiv preprint arXiv:2407.18078*, 2024.

[21] L. Zhang, J. Peng, J. Zheng, and M. Xiao, "Intelligent cloud-edge collaborations assisted energy-efficient power control in heterogeneous networks," *IEEE Trans. Wirel. Commun.*, vol. 22, no. 11, pp. 7743–7755, 2023.

[22] T. S. Rappaport, *Wireless Communications: Principles and Practice*. Pearson Education India, 2020.

[23] A. Goldsmith, *Wireless Communications*. Cambridge University Press, 2005.

[24] B. Wu, R. Zhu, Z. Zhang, P. Sun, X. Liu, and X. Jin, "dLoRA: Dynamically orchestrating requests and adapters for LoRA/LLM serving," in *Proc. OSDI*, Santa Clara, CA, USA, Jul. 2024.

[25] R. S. Sutton and A. G. Barto, *Reinforcement Learning: An Introduction*. MIT Press, 2018.

[26] Y. Peng, J. Zeng, Y. Hu, Q. Fang, and Q. Yin, "Reinforcement learning from suboptimal demonstrations based on reward relabeling," *Expert Syst. Appl.*, vol. 255, p. 124580, 2024.

[27] N. Heess, H. Soyer, A. Saxena, T. Joachims, T. Degris, P. M. Pilarski, A. J. Ballard, D. Wierstra, and J. Peters, "Learning continuous control policies by stochastic value gradients," in *Proc. NeurIPS*, Montreal, Quebec, Canada, Dec. 2015.

[28] T. Haarnoja, K. Hartikainen, P. Abbeel, and S. Levine, "Latent space policies for hierarchical reinforcement learning," in *Proc. ICML*. PMLR, 2018, pp. 1851–1860.

[29] D. N. Lee and M. R. Kosorok, "Off-policy reinforcement learning with high dimensional reward," *arXiv preprint arXiv:2408.07660*, 2024.

[30] C. Chi, S. Feng, Y. Du, Z. Xu, E. Cousineau, B. Burchfiel, and S. Song, "Diffusion Policy: Visuomotor policy learning via action diffusion," in *Proc. RSS*, Daegu, Republic of Korea, Jul. 2023.

[31] H. Abdi, "Singular value decomposition (SVD) and generalized singular value decomposition (GSVD)," in *Encyclopedia of Measurement and Statistics*, N. J. Salkind, Ed. Thousand Oaks, CA: Sage, 2007, pp. 907–912.

[32] A. Böttcher and D. Wenzel, "The frobenius norm and the commutator," *Linear Algebra Appl.*, vol. 429, no. 8-9, pp. 1864–1885, 2008.

[33] P. Henderson, R. Islam, P. Bachman, J. Pineau, D. Precup, and D. Meger, "Deep reinforcement learning that matters," in *Proc. AAAI*, New Orleans, LA, USA, Feb. 2018.

[34] M. Andrychowicz, A. Raichuk, P. Stańczyk, M. Orlowski, L. Espeholt, R. Marinier, M. Zięba, J. Kay, Y. Tassa, N. Heess *et al.*, "What matters in on-policy reinforcement learning? A large-scale empirical study," in *Proc. ICLR*, Vienna, Austria, May 2021.

[35] C. K. Williams and C. E. Rasmussen, *Gaussian processes for machine learning*. MIT Press, Cambridge, MA, 2006, vol. 2, no. 3.

[36] R. Rombach, A. Blattmann, D. Lorenz, P. Esser, and B. Ommer, "High-resolution image synthesis with latent diffusion models," in *Proc. CVPR*, New Orleans, LA, USA, Jun. 2022.

[37] J. Ho and T. Salimans, "Classifier-free diffusion guidance," *arXiv preprint arXiv:2207.12598*, 2022. [Online]. Available: https://arxiv.org/abs/2207.12598

[38] R. Socher, A. Perelygin, J. Wu, J. Chuang, C. D. Manning, A. Y. Ng, and C. Potts, "Recursive deep models for semantic compositionality over a sentiment treebank," in *Proc. EMNLP*, Seattle, WA, USA, Oct. 2013.

[39] S. Zhang, S. Roller, N. Goyal, M. Artetxe, M. Chen, S. Chen, G. Dewan, M. Diab, J. Dodge, X. L. Maestre, X. V. Lin, T. Mihaylov, M. Ott, S. Shleifer, K. Shuster, D. Simig, P. S. Koura, A. Singh, H. Schwenk, and L. Zettlemoyer, "OPT: Open pre-trained transformer language models," *arXiv preprint arXiv:2205.01068*, 2022.

[40] G. Raskutti, M. J. Wainwright, and B. Yu, "Early stopping and non-parametric regression: an optimal data-dependent stopping rule," *J. Mach. Learn. Res.*, vol. 15, no. 1, pp. 335–366, Jan. 2014.